Egypt.J.Chem. **Vol. 62**, No. 12. pp. 2183 - 2193 (2019)

Egyptian Journal of Chemistry
http://ejchem.journals.ekb.eg/

Adsorption of the Anionic Dye (Diamond Fast Brown KE) from Textile Wastewater onto Chitosan/Montmorillonite Nanocomposites

M.M. El-Defrawy[1], I.M.M. Kenawy[1], E.G. Zaki[2*], Rania M. Eltabey[1]
[1]*Chemistry Department, Faculty of Science, Mansoura University, Egypt.*
[2]*Egyptian Petroleum Research Institute (EPRI), Nasr City, Cairo, Egypt.*

A NOVEL nanocomposite chitosan/montmorillonite has been prepared by using two different weight ratios of nano-montmorillonite (Chs1 and Chs2). The structure of the prepared adsorbents has been characterized by Fourier transform infrared (FT-IR) spectroscopy, and transmission electron microscopy (TEM). The adsorption kinetics and isotherm behaviors of Diamond Fast Brown KE (DFB) dye molecules onto prepared chitosan nanocomposites had been studied and compared using pseudo-first, pseudo-second, and Langmuir, Freundlich, Dubinin-Radushkevich models, respectively. The maximum adsorption capacities of DFB according to Langmuir isotherm model were 403.23 and 375.94 mg g^{-1} for Chs1 and Chs2, respectively. Moreover, our results indicate that the adsorption mechanism can be explained by the formation of the hydrogen bond. Based on the obtained results, Chs1 and Chs2 can be successfully applied for DFB dye removal from textile wastewater.

Keywords: Chitosan, Nanocomposite, Adsorption, Textile Diamond Fast Brown KE dye.

Introduction

Dyeing wastewater has grabbed considerable public attention because of its carcinogenicity, easy accumulation in living organisms, high toxicity, and resistance to degradation [1-4]. Due to the complexity of wastewaters, and in particular the presence of the problematic azo-reactive dyes, colour removal is a major concern for the textile industries. With the introduction of strict environmental legislation regarding colour limits of industrial effluent discharge in many regions of the Middle East, the need for an effective process that efficiently remove colour is now a top priority [5]. Several methods based on distillation [6], biodegradation [7], membrane technologies [8], photocatalysis [9, 10], and adsorption [11] have been employed for the polluted water treatment. Amongst them, adsorption technique is regarded as an effective and inexpensive water remediation technique [12, 13]. Recently, multiple adsorbents have been used in the treatment of wastewater [14, 15] such as grapheme oxide, zeolites, carbon tubes, clays, polypropylene, polystyrene, polyurethane [16-18]. Bearing in mind the further extending of the advanced adsorbents application in the industrial scale, recent research is dedicated to the synthesis of adsorbents that characterized by great sorption capacity as well as favorable reusability [19, 20]. There is also other challenge concerning the treatment of dyeing wastewater which is while the anionic dyes removal has been recognized to be effective because of the positively charged surface of the sorbent occurred by protonation process [21, 22], the dyeing discharge from textile industrial use is mostly in the pH range (9-11) [23]. Therefore, there is a crucial necessity for determining of technically cost-effective, feasible, and highly efficient adsorbents for the dyeing wastewater remediation processes using alkaline conditions [24].

Chitosan (Chs) has been widely applied in wastewater treatment processes owing to its interesting characteristics like having high number of adsorption groups, biocompatibility,

*Corresponding author e-mail: chemparadise17@yahoo.com
Received 2/5/2019; Accepted 11/5/2019
DOI: 10.21608/ejchem.2019.12467.1775

high adsorption capacity, abundance, macromolecular structure, non-toxicity, low cost, biodegradability, selectivity, and versatility [25, 26]. Several materials have been employed in order to synthesize Chs composites such as montmorillonite due to their large specific area, the possibility of interlayer expansion, and high cation exchange capacity simple and green preparation methods in addition to attractive chemical and physical properties [27, 28]. Whereas montmorillonite provides good affinity for cationic dyes [29], it often offers little capacity towards anionic dyes due to its negatively charged surface [30, 31]. Hence, the montmorillonite modification with polymers may alter its chemical or physical characterestics as well as enhance its affinity for anionic dyes.

In current study, chitosan montmorillonite nanocomposites have been synthesized using glutaraldehyde and ammonium hydroxide as crosslinking agents with montmorillonite (wt% 0.56, and 11.3% based on Chs) in order to get adsorbents applicable for Diamond Fast Brown KE (DFB) dye removal from aqueous solution. The prepared nanocomposites have been characterized in order to explain the adsorption behavior. Moreover, the reusability of adsorbents in addition to adsorption kinetics, isotherms, initial pH, and contact time effect of DFB on Chs nanocomposites have been studied. Furthermore, the mechanism of adsorption process has been discussed.

Procedures of the Experiment

Materials

All chemicals including Chs (MW. =100 kDa) with a degree of deacetylation 93%, nano-montmorillonite, glutaraldehyde 25%, and ammonium hydroxide solution (NH_4OH) 33% were provided by Sigma-Aldrich Trading Co., Ltd. Diamond fast brown KE (DFB) dye (Fig. 1) was purchased from the Dye Star Company, Brazil. An amount of DFB was dissolved in double distilled water to prepare a stock solution at 1000 mg L^{-1}, while the working solutions were prepared by dilution of the stock solution.

Characterization

The chemical structure of the dye has been shown in Fig 1. FTIR (Perkin Elmer Spectrum BX) absorption spectra of the prepared nanocomposites were measured over the range of 4000–400 cm^{-1}. The morphology analysis of these nanocomposites was carried out by transmission electron microscope (TEM, Hitachi H-800 at 200 kV, Japan). The point of zero charge (pH_{PZC}) onto the surface of the two adsorbents was investigated by batch equilibrium method as described in previous article [32]. The DFB concentrations were determined using a Jasco UV-Vis spectrophotometer (model V-530, Japan) at a wavelength of 530 nm.

Preparation of the chitosan nanocomposites

The chitosan montmorillonite nanocomposites have been prepared using the following procedure: 1.61 g of Chs and 200 mL of acetic acid (5%) were mixed in a 250 mL beaker till complete dissolution. Then, different amounts of nano-montmorillonite clay of 0.56%, and 11.3% were added to Chs solution producing two different samples. After 12 hours stirring at room temperature, 0.01 mole of glutaraldehyde was further added to each reaction mixture and heated under reflux conditions at 80 °C. In order to crosslink ammonia; each product obtained in the previous step was stirred with 0.01 mole of NH_4OH solution at 100 °C, to form a gelatinous precipitate which was washed carefully several times with doubly distilled water and then dried in air. The two samples were ground in an agate mortar and denoted as Chs1, and Chs2, respectively. Fig. 2 depicts the chemical structure of the prepared nanocomposites.

Adsorption studies

The initial pH effect was carried out by mixing 20 mg of each prepared adsorbent and 100 mL of DFB (100 mg L^{-1}); the initial pH was adjusted using a buffer solution (4–10). This pH range has been selected in order to avoid dye degradation which occurred at strong acidic medium. Kinetic studies were conducted with fixed amounts of each adsorbent 20 mg and initial DFB concentration 100 mg L^{-1} at time intervals (30-240 min). The isotherm studies were performed by agitating 25 mL DFB solution at pH 8 for 120 min.

Results and Discussion

FT-IR

FTIR investigation of prepared nanocomposites, as seen in Fig. 3, proves the presence of strong broad absorption peaks around 3600–3200 cm^{-1} which may be associated with the intermolecular hydrogen bonds of the polysaccharide, the extension vibration of the –NH, and the stretching vibration of –OH. Moreover, there are weak peaks at 1672 and 1541 cm^{-1} which attribute to amide I and amide II, respectively [33]. In addition, montmorillonite displays peaks

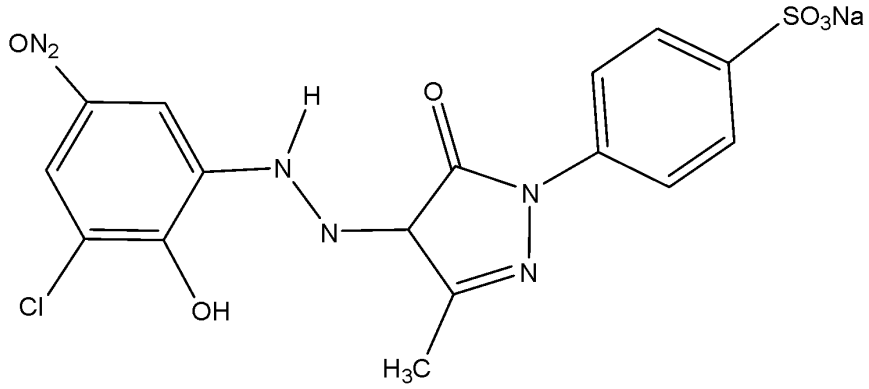

Fig. 1. Chemical structure of Diamond Fast Brown KE (DFB).

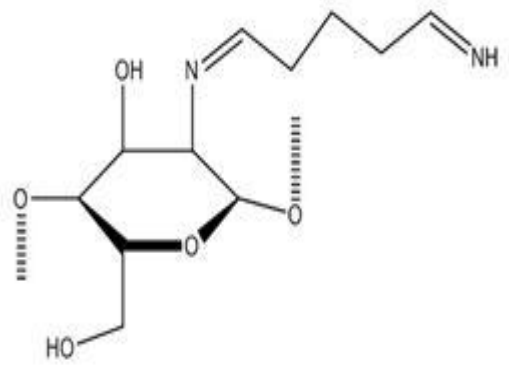

Fig. 2. Proposed chemical structure of prepared adsorbents.

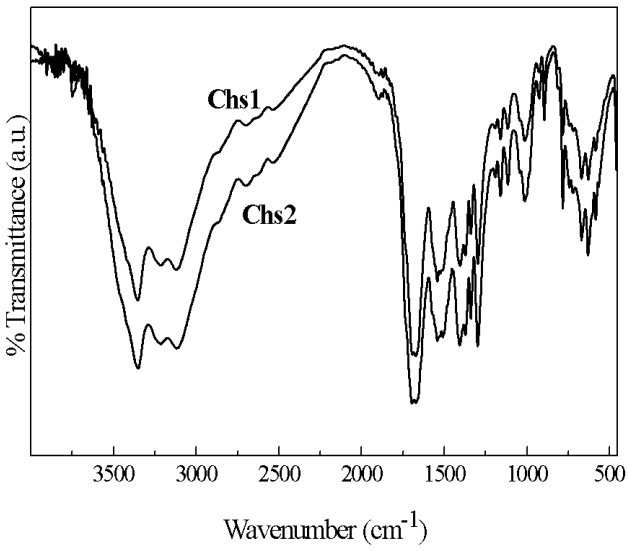

Fig. 3. FTIR spectra for Chs1 and Chs2.

at 458 and 583 cm^{-1} corresponded to the Si-O-Mg and Si-O-Al bending frequencies, while a peak at 1013 cm^{-1} attributes to Si-O stretching vibrations [34-36]. As further seen in Fig. 3, the intensity of the peaks attached to the intercalated Chs methylene (2701 cm^{-1}) groups and (C–H bending on methyl (1406 cm^{-1}) and methylene (1372 cm^{-1}) groups) and (C–H stretching on methyl (2860 cm^{-1}), increase with corresponding increase in the wt% of montmorillonite [37].

TEM

Fig. 4 reveals the TEM images of both prepared adsorbents. The dark lines pointed out the well delaminated nano-montmorillonite layers which were stabilized within the crosslinked polymer matrix, whereas the bright zone reflected the intercalated Chs matrix. Sizes were less than 100 nm, so it could be assumed that both prepared composites were nanocomposite materials [38-40].

Point of zero charge (pHPZC).

The isoelectric point of Chs is pH 6.5. Under acidic levels, the –OH and $–NH_2$ groups of Chs are protonated by H^+ ions of the acidic medium [41]. On the contrary, under basic levels, Chs's –OH and $–NH_2$ groups are deprotonated, which in turn leads to an additional negative surface charge [42-45]. Regarding our study, the pH_{PZC} of the prepared adsorbents became more negative at much lower pH levels upon increasing of nano-montmorillonite content added to Chs, which referred to more chemical stability at acidic medium [28]. pH_{PZC} are 5.81 and 5.49 for Chs1 and Chs2, respectively. At a $pH<pH_{PZC}$, the nanocomposites' surfaces are positively charged, while, as the pH is more than pH_{PZC}, the surface of the prepared adsorbents is negatively charged [46]. Fig. 5 displays the point of zero charge of the prepared nanocomposites.

Effect of initial pH

The effect of initial pH on DFB adsorption has been studied by stirring 25 mL mixture of DFB (100 mg L^{-1}) and 20 mg of each adsorbent at the pre-mentioned pH values, and equilibrium adsorption (q_e) was plotted against the pH. From Fig. 6, we can see that the adsorption of DFB on each prepared adsorbent is pH-independent. Therefore, the alkaline pH 8 has been chosen for the next experiments to be performed at, which is near the pH range of the dyeing discharge from textile industrial use as mentioned in section 1.

Effect of contact time

In order to determine the influence of the optimal contact time, the adsorption behavior of DFB on the adsorbents Chs1 and Chs2 at (30°C) has been studied (Fig.7). The experimental conditions were at 6 different times (min) of 5, 15, 30, 60, 120, and 240 with an adsorbent dosage of 0.02 g in 25 mL solution with an initial DFB concentration of 100 mg L^{-1} at pH=8. Fig.7 shows the adsorption capacity of DFB by the adsorbents. As can be seen in this figure, the adsorption rate increases and then remains constant at 120 min. This behavior is observed in both adsorbents but the adsorbent Chs1 exhibits a greater adsorption. Therefore, 120 min was selected as the equilibrium time (optimal value) for the saturation of both adsorbents of DFB molecules.

Kinetics Analysis

In the kinetics studies, the initial pH was

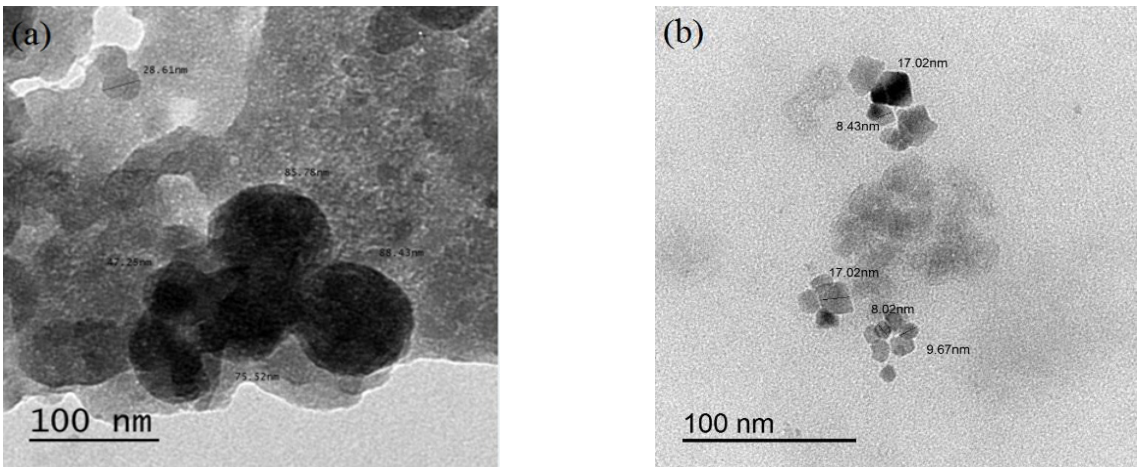

Fig. 4. TEM images of (a) Chs1, and (b) Chs2.

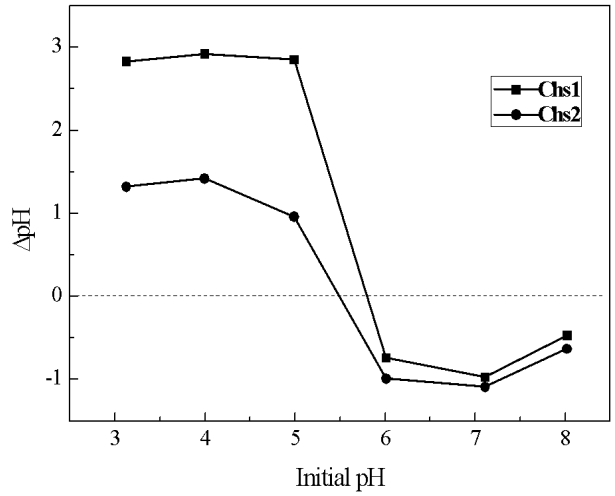

Fig. 5. Plot of point of zero charge (pHPZC) of Chs1 and Chs2.

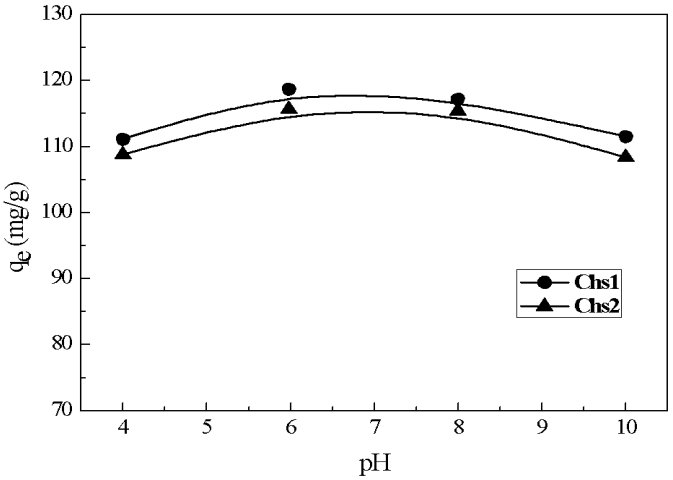

Fig. 6. Effect of pH on the adsorption of DFB onto Chs1 and Chs2.

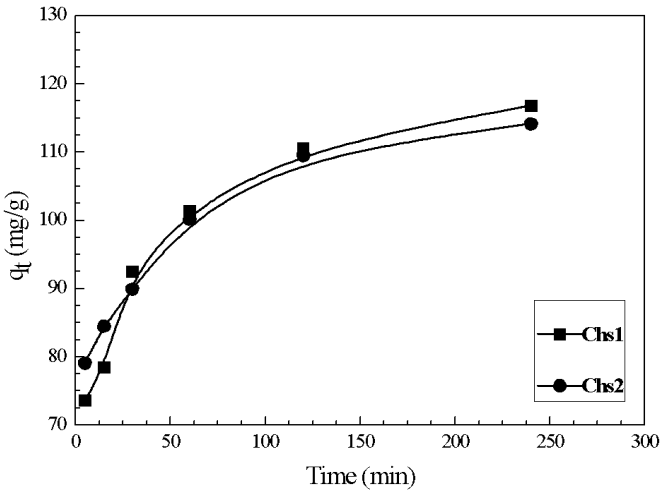

Fig. 7. Effect of contact time of DFB dye adsorption onto prepared nanocomposites.

adjusted at 8 and the initial DFB concentration was of 100 mg L^{-1} at 30°C, applying the prepared nanocomposites. The adsorption kinetics have been explained by the fitting of the models of pseudo-first (Eq. 1) and pseudo-second order (Eq. 2) to the experimental data [47,48],

$$q_t = q_1(1-\exp(-k_1 t)) \quad (1)$$

$$q_t = t / (1/k_2 q_2^2) + (t/q_2) \quad (2)$$

Here, q_t (mg g^{-1}) is the amount of DFB sorbed at (t) time, k_1 (min^{-1}) and k_2 (g $mg^{-1}min^{-1}$) are the rate constants of pseudo-first and pseudo-second order kinetic models, respectively, q_1 and q_2 (mg g^{-1}) are the theoretical values of the adsorption capacity. Fig. 8a, and b display the experimental curves of pseudo-first and pseudo-second order adsorption kinetic models, respectively, for DFB onto nanocomposites. The constants of the studied kinetic models are given in Table 1. From Table 1, the pseudo-second order kinetic model is the most appropriate model representing the adsorption kinetics of DFB dye, for both nanocomposites, owing to the highest R^2 values (R^2> 0.99).

Adsorption Isotherm Models

In this work, two adsorption isotherm models, Langmuir and Freundlich, have been applied to analyze the mechanism of adsorption of DFB dye on the prepared adsorbents [49]. Langmuir isotherm model hypotheses monolayer adsorption on the surface of adsorbent with fixed active sites of adsorption and given as depicted in (Eq. 3),

$$C_e/q_e = C_e/q_m + 1/ q_m K_L \quad (3)$$

Here, q_m (mg g^{-1}) is the maximum adsorption capacity of nanocomposites, and K_L (L mg^{-1}) is the Langmuir constant

A straight line attained from the graph of C_e/q_e versus C_e points out $1/q_m$ and $1/K_L\ q_m$ as the slope

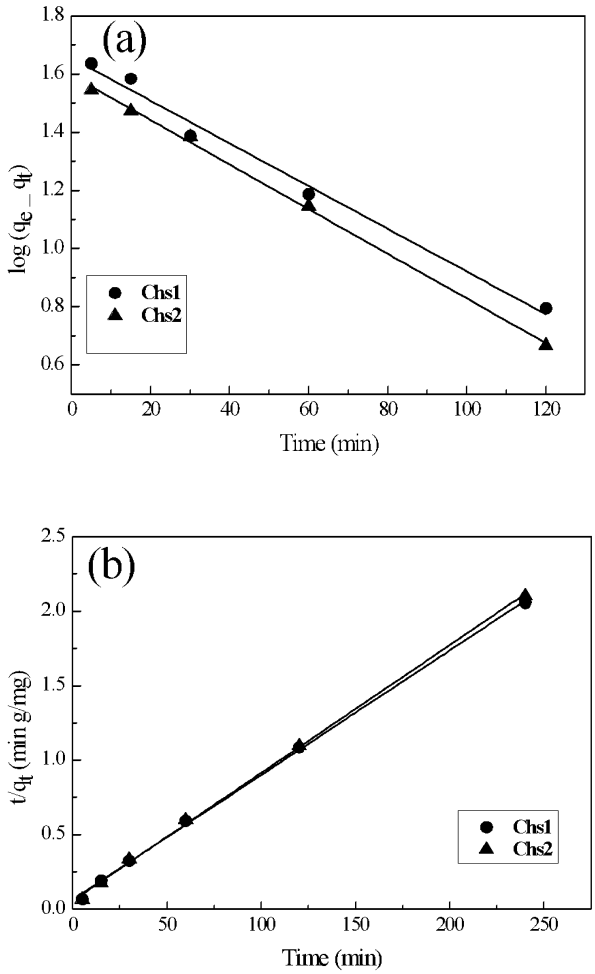

Fig. 8. Linear fitting of (a) pseudo-first, and (b) pseudo-second models for both adsorbents.

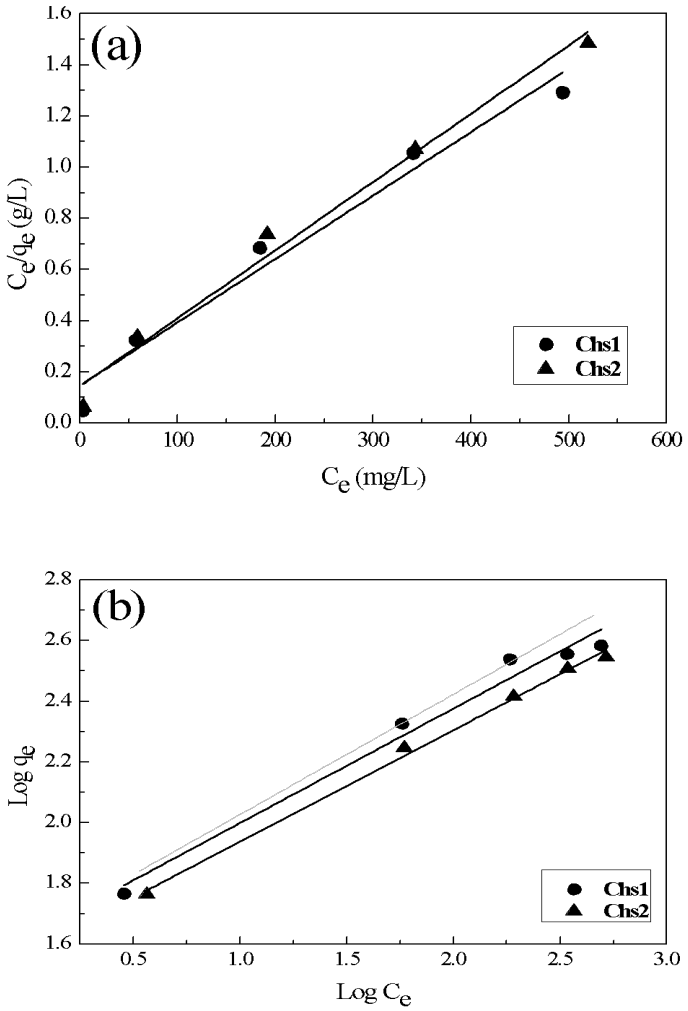

Fig. 9. Plot of (a) Langmuir adsorption isotherm, and (b) Freundlich adsorption isotherm for adsorption of DFB onto both adsorbents.

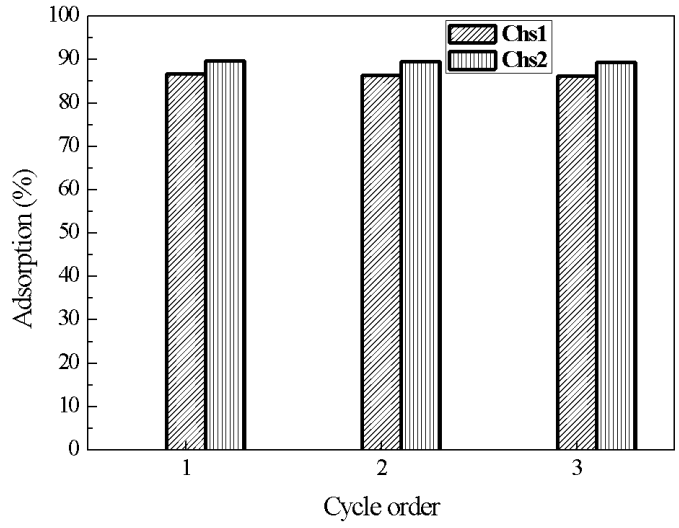

Fig. 10. Reusability efficiencies of both adsorbents in three cycles of adsorption-desorption cycles.

and intercept, respectively [50, 51]. However, the Freundlich adsorption isotherm model suggests that adsorption occurs on a heterogeneous surface and is expressed by (Eq. 4) [52, 53],

$$\text{Log}\, q_e = \log K_F + 1/n \,\text{Log}\, C_e \quad (4)$$

Here, K_F (mg g^{-1}), and 1/n are the Freundlich model constants. The adsorption isotherms had been analyzed by the Langmuir and Freundlich isotherm models. The calculated constant values of the two studied models are given in Table 2. R^2 values regarding to Langmuir model are 0.973, 0.995, while their values according to Freundlich are 0.963, 0.981, for Chs1 and Chs2, respectively. Hence, both models sufficiently predicted well the adsorption of DFB onto the prepared nanocomposites, whereas, the Langmuir equation produced a slightly better fitting to the obtained data, which is displayed in Fig. 9, indicating the monolayer adsorption nature. The adsorption capacity of DFB had been theoretically calculated at 403.23 and 375.94 mg g^{-1} for Chs1 and Chs2, respectively.

In order to illustrate the mechanism of DFB adsorption onto both adsorbents, Dubinin-Radushkevich (D-R) isotherm has been applied. This isotherm is considered to be more general than Langmuir adsorption isotherm because it supposes neither a constant adsorption potential nor a homogeneous surface. This model has been widely applied to recognize physical or chemical adsorption. The linearized form of D-R adsorption isotherm model is expressed by (Eq. 5) [54]:

$$\ln q_e = \ln q_{D\text{-}R} - \beta \varepsilon^2 \quad (5)$$

Where, $q_{D\text{-}R}$ is theoretical saturation capacity of nanocomposites (mg g^{-1}), and β is a constant associated with the adsorption mean free energy per mole of the dye ($mol^2\ kJ^{-2}$). Ɛ, Polanyi potential, is a logarithmic function of concentration and is expressed by the following:

$$\varepsilon = RT \ln(1 + 1/C_e) \quad (6)$$

Where, T and R are the temperature in Kelvin and gas constant, respectively. $E_{D\text{-}R}$, the adsorption apparent energy for transferring of the dye from infinity in the solution to the surface of nanocomposites, has been calculated from β values using (Eq. 7):

$$E_{D\text{-}R} = \sqrt{1/2\beta} \quad (7)$$

The values of average apparent energy are calculated at 0.428 and 0.347 kJ mol^{-1} ($E_{D\text{-}R}$<8.0 kJ mol^{-1}) for Chs1 and Chs2, respectively (Table 2), which refer to the physical nature of DFB adsorption on each of prepared adsorbents [55].

Desorption and Reuse

The desorption process of DFB from the nanocomposites has been performed by NaOH with a concentration of 1 mole L^{-1}. The presence of NaOH resulted in an elevation of the pH value and, consequently, number of OH^- ions would highly increase leading to a great repulsion power between OH^- ions and the anions which act as binding sites on the adsorbents. This led to the removal of the anionic dye from the chitosan nanocomposites. Three cycles of adsorption/desorption were conducted to detect if the prepared nanocomposites could be reused. Fig. 10 displays the removal percent values in different cycles of adsorption/regeneration. It is obvious that the nanocomposites offer a good performance in the reuse, which ascribes to the fact that the chitosan nanocomposites' sorption capacities decline only by 10% after three cycles of adsorption/desorption.

Proposed adsorption mechanism

As mentioned in section 3.3, all experiments have been conducted at pH 8 (>pH_{PZC}) which means that the surface of adsorbents is negatively charged making electrostatic attraction hardly acceptable to illustrate the mechanism of adsorption. Hydrogen bonding is regarded as one of the most important mechanisms of adsorption for separating or removing different types of molecules [56]. According to previously described results, the mechanism controlling DFB adsorption on the prepared nanocomposites at solution pH 8 (Fig. 11), is due to hydrogen bonding between –Cl, –N, and –O containing functional groups of DFB and H atoms from =NH, and –OH groups of prepared nanocomposites. These findings agree well with result obtained from D-R isotherm model and desorption studies.

Conclusion

The modification of chitosan by different weight ratios of nano-montmorillonite as well as crosslinking with glutaraldehyde/ NH_4OH for use as adsorbents of DFB was investigated. The prepared nanocomposites have been characterized by FT-IR and TEM. The Langmuir isotherm model represented the system equilibrium and the maximum adsorption capacities according to Langmuir model were 403.23 and 375.94 mg g^{-1} for Chs1 and Chs2, respectively, at 30°C. The

pseudo-second order kinetic model was best fitted to the adsorption kinetics data. The eluent NaOH 1 mol L^{-1} was applied for the regeneration of the adsorbents, three cycles of adsorption/desorption were possible.

References

1. Akhtar M. F., Ashraf M., Javeed A., Anjum A. A., Sharif A., Saleem A., Akhtar B., Khan A. M., Altaf I. Toxicity appraisal of untreated dyeing industry wastewater based on chemical characterization and short term bioassays, *Bulletin of Environmental Contamination and Toxicology,* **96,** 502-507 (2016).

2. Gupta V. Application of low-cost adsorbents for dye removal–A review, *Journal of Environmental Management*, **90,** 2313-2342 (2009).

3. Metwally B. S., El-Sayed A. A., Radwan E. K., Hamouda A. S., El-Sheikh M., Salama M. Fabrication, Characterization, and Dye Adsorption Capability of Recycled Modified Polyamide Nanofibers, *Egyptian Journal of Chemistry*, **61,** 867-882 (2018).

4. Haroun A., Mashaly H., Helmy H., Kamel M. Kinetic study of gelatin/chitosan based nanocomposites for acid red 150 dye adsorption using ultrasonic energy, *Egypt J Chem*. https://doi.org/10.21608/ejche m, 1007 (2017).

5. Al-Ghouti M., Khraisheh M., Allen S., Ahmad M. The removal of dyes from textile wastewater: a study of the physical characteristics and adsorption mechanisms of diatomaceous earth, *Journal of Environmental Management,* **69,** 229-238 (2003).

6. Criscuoli A., Zhong J., Figoli A., Carnevale M., Huang R., Drioli E. Treatment of dye solutions by vacuum membrane distillation, *Water Research,* **42,** 5031-5037 (2008).

7. Kulkarni A. N., Kadam A. A., Kachole M. S., Govindwar S. P., Lichen P. A novel system for biodegradation and detoxification of disperse dye Solvent Red 24, *Journal of Hazardous Materials,* **276,** 461-468 (2014).

8. Alventosa-deLara E., Barredo-Damas S., Alcaina-Miranda M., Iborra-Clar M. Ultrafiltration technology with a ceramic membrane for reactive dye removal: optimization of membrane performance, *Journal of Hazardous Materials,* **209,** 492-500 (2012).

9. Ameen S., Akhtar M. S., Seo H.-K., Shin H.-S. Solution-processed CeO2/TiO2 nanocomposite as potent visible light photocatalyst for the degradation of bromophenol dye, *Chemical Engineering Journal,* **247,** 193-198 (2014).

10. Zhou Y., Gu X., Zhang R., Lu J. Influences of various cyclodextrins on the photodegradation of phenol and bisphenol A under UV light, *Industrial & Engineering Chemistry Research,* **54,** 426-433 (2015).

11. Garg V., Gupta R., Yadav A. B., Kumar R. Dye removal from aqueous solution by adsorption on treated sawdust, *Bioresource Technology,* **89,** 121-124 (2003).

12. Rafatullah M., Sulaiman O., Hashim R., Ahmad A. Adsorption of methylene blue on low-cost adsorbents: a review, *Journal of Hazardous Materials,* **177,** 70-80 (2010).

13. Waly A., Khedr M., Ali H., Riad B., Ahmed I. Synthesis and Characterization of Ion Exchanger based on Waste Cotton for Dye Removal from Wastewater, *Egyptian Journal of Chemistry,* **62,** 451-468 (2019).

14. Ramakrishna K. R., Viraraghavan T. Dye removal using low cost adsorbents, *Water Science and Technology,* **36,** 189-196 (1997).

15. Zhou Y., Zhang R., Gu X., Lu J. Adsorption of divalent heavy metal ions from aqueous solution by citric acid modified pine sawdust, *Separation Science and Technology,* **50,** 245-252 (2015).

16. Sanghi R., Bhattacharya B. Review on decolorisation of aqueous dye solutions by low cost adsorbents, *Coloration Technology,* **118,** 256-269 (2002).

17. Yagub M. T., Sen T. K., Afroze S., Ang H. M. Dye and its removal from aqueous solution by adsorption: a review, *Advances in Colloid and Interface Science,* **209,** 172-184 (2014).

18. Huang W., Hu Y., Li Y., Zhou Y., Niu D., Lei Z., Zhang Z. Citric acid-crosslinked β-cyclodextrin for simultaneous removal of bisphenol A, methylene blue and copper: the roles of cavity and surface functional groups, *Journal of the Taiwan Institute of Chemical Engineers,* **82,** 189-197 (2018).

19. Lu F., Huang C., You L., Wang J., Zhang Q. Magnetic hollow carbon microspheres as a reusable adsorbent for rhodamine B removal, *RSC Advances,* **7,** 23255-23264 (2017).

20. Orlandi G., Cavasotto J., Machado Jr F. R., Colpani G. L., Dal Magro J., Dalcanton F., Mello J. M.,

Fiori M. A. An adsorbent with a high adsorption capacity obtained from the cellulose sludge of industrial residues, *Chemosphere*, **169,** 171-180 (2017).

21. Pal S., Patra A. S., Ghorai S., Sarkar A. K., Mahato V., Sarkar S., Singh R. Efficient and rapid adsorption characteristics of templating modified guar gum and silica nanocomposite toward removal of toxic reactive blue and Congo red dyes, *Bioresource Technology,* **191,** 291-299 (2015).

22. Liu S., Ding Y., Li P., Diao K., Tan X., Lei F., Zhan Y., Li Q., Huang B., Huang Z. Adsorption of the anionic dye Congo red from aqueous solution onto natural zeolites modified with N, N-dimethyl dehydroabietylamine oxide, *Chemical Engineering Journal,* **248,** 135-144 (2014).

23. Shen C., Shen Y., Wen Y., Wang H., Liu W. Fast and highly efficient removal of dyes under alkaline conditions using magnetic chitosan-Fe (III) hydrogel, *Water Research,* **45,** 5200-5210 (2011).

24. Hui M., Shengyan P., Yaqi H., Rongxin Z., Anatoly Z., Wei C. A highly efficient magnetic chitosan "fluid" adsorbent with a high capacity and fast adsorption kinetics for dyeing wastewater purification, *Chemical Engineering Journal,* **345,** 556-565 (2018).

25. Vakili M., Deng S., Li T., Wang W., Wang W., Yu G. Novel crosslinked chitosan for enhanced adsorption of hexavalent chromium in acidic solution, *Chemical Engineering Journal,* **347,** 782-790 (2018).

26. Hamouda A. S., Ahmed S. A., Mohamed N., Khalil M. Adsorption of Chromium (Vi) from Aqueous Solution by Glycine Modified Cross-linked Chitosan Resin, *Egyptian Journal of Chemistry,* **61,** 799-812 (2018).

27. Jaber M., Georgelin T., Bazzi H., Costa-Torro F., Lambert J.-F. o., Bolbach G. r., Clodic G. Selectivities in adsorption and peptidic condensation in the (arginine and glutamic acid)/ montmorillonite clay system, *The Journal of Physical Chemistry C,* **118,** 25447-25455 (2014).

28. Pereira F. A., Sousa K. S., Cavalcanti G. R., França D. B., Queiroga L. N., Santos I. M., Fonseca M. G., Jaber M. Green biosorbents based on chitosan-montmorillonite beads for anionic dye removal, *Journal of Environmental Chemical Engineering,* **5,** 3309-3318 (2017).

29. Wang L., Zhang J., Wang A. Removal of methylene blue from aqueous solution using chitosan-g-poly (acrylic acid)/montmorillonite superadsorbent nanocomposite, *Colloids and Surfaces A: Physicochemical and Engineering Aspects,* **322,** 47-53 (2008).

30. Fournier F., de Viguerie L., Balme S., Janot J.-M., Walter P., Jaber M. Physico-chemical characterization of lake pigments based on montmorillonite and carminic acid, *Applied Clay Science,* **130,** 12-17 (2016).

31. Thangaraj V., Bussiere J., Janot J. M., Bechelany M., Jaber M., Subramanian S., Miele P., Balme S. Fluorescence quenching of sulforhodamine dye over graphene oxide and boron nitride nanosheets, *European Journal of Inorganic Chemistry,* **2016** 2125-2130 (2016).

32. Lazarević S., Janković-Častvan I., Jovanović D., Milonjić S., Janaćković D., Petrović R. Adsorption of Pb2+, Cd2+ and Sr2+ ions onto natural and acid-activated sepiolites, *Applied Clay Science,* **37** 47-57 (2007).

33. Zhou Q., Gao Q., Luo W., Yan C., Ji Z., Duan P. One-step synthesis of amino-functionalized attapulgite clay nanoparticles adsorbent by hydrothermal carbonization of chitosan for removal of methylene blue from wastewater, *Colloids and Surfaces A: Physicochemical and Engineering Aspects,* **470,** 248-257 (2015).

34. Silva M. M., Oliveira M. M., Avelino M. C., Fonseca M. G., Almeida R. K., Silva Filho E. C. Adsorption of an industrial anionic dye by modified-KSF-montmorillonite: Evaluation of the kinetic, thermodynamic and equilibrium data, *Chemical Engineering Journal,* **203,** 259-268 (2012).

35. Hassanien M. M., Abou-El-Sherbini K. S., Al-Muaikel N. S. Immobilization of methylene blue onto bentonite and its application in the extraction of mercury (II), J*ournal of Hazardous Materials,* **178,** 94-100 (2010).

36. Kenawy E.-R., Ghfar A. A., Wabaidur S. M., Khan M. A., Siddiqui M. R., Alothman Z. A., Alqadami A. A., Hamid M. Cetyltrimethylammonium bromide intercalated and branched polyhydroxystyrene functionalized montmorillonite clay to sequester cationic dyes, *Journal of Environmental Management,* **219,** 285-293 (2018).

37. Teimouri A., Nasab S. G., Habibollahi S., Fazel-Najafabadi M., Chermahini A. N. Synthesis and

characterization of a chitosan/montmorillonite/ZrO 2 nanocomposite and its application as an adsorbent for removal of fluoride, *RSC Advances,* **5,** 6771-6781 (2015).

38. Gogoi P., Thakur A. J., Devi R. R., Das B., Maji T. K. A comparative study on sorption of arsenate ions from water by crosslinked chitosan and crosslinked chitosan/MMT nanocomposite, *Journal of Environmental Chemical Engineering,* **4,** 4248-4257 (2016).

39. Reddy A. B., Manjula B., Jayaramudu T., Sadiku E., Babu P. A., Selvam S. P. 5-Fluorouracil loaded chitosan–PVA/Na+ MMT nanocomposite films for drug release and antimicrobial activity, *Nano-Micro Letters,* **8,** 260-269 (2016).

40. Luo J., Han G., Xie M., Cai Z., Wang X. Quaternized chitosan/montmorillonite nanocomposite resin and its adsorption behavior, *Iranian Polymer Journal*, **24,** 531-539 (2015).

41. Rinaudc M., Pavlov G., Desbrieres J. Solubilization of chitosan in strong acid medium, *International Journal of Polymer Analysis and Characterization,* **5,** 267-276 (1999).

42. Kosmulski M. The pH-dependent surface charging and points of zero charge: V. Update, *Journal Of Colloid and Interface Science,* **353,** 1-15 (2011).

43. Marques Neto J. d. O., Bellato C. R., Milagres J. L., Pessoa K. D., Alvarenga E. S. d. Preparation and evaluation of chitosan beads immobilized with Iron (III) for the removal of As (III) and As (V) from water, *Journal of the Brazilian Chemical Society,* **24,** 121-132 (2013).

44. He C., Shi L., Lou S., Liu B., Zhang W., Zhang L. Synthesis of spherical magnetic calcium modified chitosan micro-particles with excellent adsorption performance for anionic-cationic dyes, *International Journal of Biological Macromolecules,* **128,** 593-602 (2019).

45. Minisy I., Salahuddin N., Ayad M. Chitosan/polyaniline hybrid for the removal of cationic and anionic dyes from aqueous solutions, *Journal of Applied Polymer Science,* **136,** 47056 (2019).

46. Banerjee S., Chattopadhyaya M. Adsorption characteristics for the removal of a toxic dye, tartrazine from aqueous solutions by a low cost agricultural by-product, *Arabian Journal of Chemistry*, **10,** S1629-S1638 (2017).

47. Gonçalves J. O., Silva K. A., Dotto G. L., Pinto L. A. Adsorption Kinetics of Dyes in Single and Binary Systems Using Cyanoguanidine-Crosslinked Chitosan of Different Deacetylation Degrees, *Journal of Polymers and the Environment,* **26** 2401-2409 (2018).

48. Aboelenin R., Kheder S., Farag H., El Nabarawy T. Removal of Cationic Neutral Red Dye from Aqueous Solutions Using Natural and Modified Rice Straw, *Egyptian Journal of Chemistry*, **60** 577-589 (2017).

49. Ho Y.-S., Chiu W.-T., Wang C.-C. Regression analysis for the sorption isotherms of basic dyes on sugarcane dust, *Bioresource Technology,* **96** 1285-1291 (2005).

50. Khalid A., Zubair M., A comparative study on the adsorption of Eriochrome Black T dye from aqueous solution on graphene and acid-modified graphene, *Arabian Journal for Science and Engineering,* **43,** 2167-2179 (2018).

51. El-Shamy A., Farag H., Saad W. Comparative Study of Removal of Heavy Metals from Industrial Wastewater Using Clay and Activated Carbon in Batch and Continuous Flow Systems, *Egyptian Journal of Chemistry,* **60,** 2065-2075 (2017).

52. Bhullar N., Kumari K., Sud D. A biopolymer-based composite hydrogel for rhodamine 6G dye removal: its synthesis, adsorption isotherms and kinetics, *Iranian Polymer Journal,* 1-9 (2018).

53. Shouman M. A. H., Attia A. A. M., Fathy N. A., Abbas K. M., Sayyah S. M., Bolis A. Sequestration of Methylene Blue and Lead ions by MWCNT Modified with Polyconducting Polymers, *Egyptian Journal of Chemistry,* **60,** 221-241 (2017).

54. Chaudhry S. A., Ahmed M., Siddiqui S. I., Ahmed S. Fe (III)–Sn (IV) mixed binary oxide-coated sand preparation and its use for the removal of As (III) and As (V) from water: application of isotherm, kinetic and thermodynamics, *Journal of Molecular Liquids,* **224,** 431-441 (2016).

55. Chaudhry S. A., Khan T. A., Ali I. Zirconium oxide-coated sand based batch and column adsorptive removal of arsenic from water: Isotherm, kinetic and thermodynamic studies, E*gyptian Journal of Petroleum*, **26,** 553-563 (2017).

56. Ahmed I., Jhung S. H. Applications of metal-organic frameworks in adsorption/separation processes via hydrogen bonding interactions, *Chemical Engineering Journal,* **310,** 197-215 (2017).